Fabrication and characterization of high performance sub-millimetric InGaP/InGaAs/Ge solar cells

Corentin Jouanneau, Thomas Bidaud, Paul Ferreol, Benjamin Breton, Gwenaelle Hamon, Maxime Darnon

Solar Energy Materials & Solar Cells 282 (2025) 113320

Contents lists available at ScienceDirect

Solar Energy Materials and Solar Cells

journal homepage: www.elsevier.com/locate/solmat

Fabrication and characterization of high performance sub-millimetric InGaP/InGaAs/Ge solar cells

Corentin Jouanneau [a,b,*], Thomas Bidaud [a,b], Paul Ferreol [a,b], Benjamin Breton [a,b], Gwenaelle Hamon [a,b], Maxime Darnon [a,c]

[a] Laboratoire Nanotechnologies Nanosystèmes (LN2)–CNRS, Université de Sherbrooke, 3000, boulevard de l'Université, Sherbrooke, Québec, J1K 0A5, Canada
[b] Institut Interdisciplinaire d'Innovation Technologique (3IT), Université de Sherbrooke, 3000, boulevard de l'Université, Sherbrooke, Québec, J1K 0A5, Canada
[c] Laboratoire Hubert Curien, Université de Lyon, UMR CNRS 5516, 42000 St Etienne, France

ARTICLE INFO

Keywords:
III–V semiconductors
Micro-CPV
Micro-cells
Triple junctions solar cells
Micro-fabrication

ABSTRACT

Micro-Concentrator photovoltaics modules promise to overcome the limitations of CPV such as thermal losses or resistive losses. Miniaturization involves new challenges in the field of cells fabrication, particularly the management of perimeter recombinations. In this paper, sub-millimetric InGaP/InGaAs/Ge solar cells with high performances are fabricated. We report record open circuit voltage of 2.39 V and 2.28 V for cells with mesa area of 0.25 mm^2 and 0.04 mm^2 respectively, indicating excellent sidewall passivation. Individual assessment of sub-cells non-radiative losses indicates that the top cell is the most impacted by perimeter recombinations.

1. Introduction

The use of III–V materials enables to obtain semi-conductors with tunable bandgaps. This property can be used in the photovoltaic field to target different spectral ranges. III–V materials can absorb wavelengths ranging from mid-infrared to ultraviolet region. Superposition of III–V's layers (multijunction) therefore allows to increase the spectral range absorbed by solar cells compared to silicon cells. Therefore, multijunction solar cells holds the highest efficiency conversion among photovoltaic cells (39.5%) [1].

The major drawback of these materials is their cost, typically more than 2 orders of magnitude more expensive than technology deployed on a large scale [2]. To manage this problem, concentrated photovoltaic (CPV) technology promises to reduce costs by adding concentration optics to solar cells, thereby limiting the uses of III–V materials. Another advantage of light concentration is the increase in cell performance, since open circuit voltage (V_{oc}) increases logarithmically with concentration.

CPV holds records efficiency conversion among photovoltaic technologies [3–5]. For triple junction, commercial solar cells (InGaP/GaAs/InGaAs) reach an efficiency above 44.4% under 302 suns (AM1.5D) concentration [3,6]. However, due to decrease of flat panel Silicon-based photovoltaics costs, CPV has difficulties to be competitive. The most promising way towards CPV competitivity is miniaturization [7–9]. Several advantages are expected: better thermal management [7,10], less resistive losses [7,8,10–13] and better compactness [10,14–16].

Even though μ-CPV appears to be a good alternative to conventional CPV, numerous manufacturing challenges remain to be overcome, especially for the fabrication of high efficiency sub-millimeter solar cells. The reduction in cell size, down to sub-millimeter dimensions, leads to an increase in perimeter recombinations [12,13,17,18]. These recombinations have an impact on V_{oc} and thus on cell performances. The way in which the cells are isolated must therefore be adapted to generated as few defect as possible. Plasma dicing is known to generate fewer defect than saw dicing [13], its positive effect on V_{oc} has also been demonstrated [19,20]. Moreover, the addition of hydrogen to the plasma results in passivation of the sidewalls, which increases the V_{oc} [21].

In this article, solar cells of different shapes and sizes (from 12.25 mm^2 down to 0.01 mm^2 mesa area) are fabricated using a process based on plasma etching for cell isolation and singulation. These cells are then electrically characterized under AM1.5D spectrum. The dependency of V_{oc} on perimeter-to-area ratio (P/A) is then presented and compared with the state of the art [12,13]. Sub-cells of different sizes are then manufactured to assess V_{oc} losses sub-cell by sub-cell. Theoretical radiative V_{oc} of each sub-cell in triple junction configuration has

* Correspondence to: 3000, boulevard de l'Université, Sherbrooke, Québec, J1K0A5, Canada.
E-mail address: corentin.jouanneau@usherbrooke.ca (C. Jouanneau).

https://doi.org/10.1016/j.solmat.2024.113320
Received 26 September 2024; Received in revised form 13 November 2024; Accepted 21 November 2024
Available online 3 December 2024

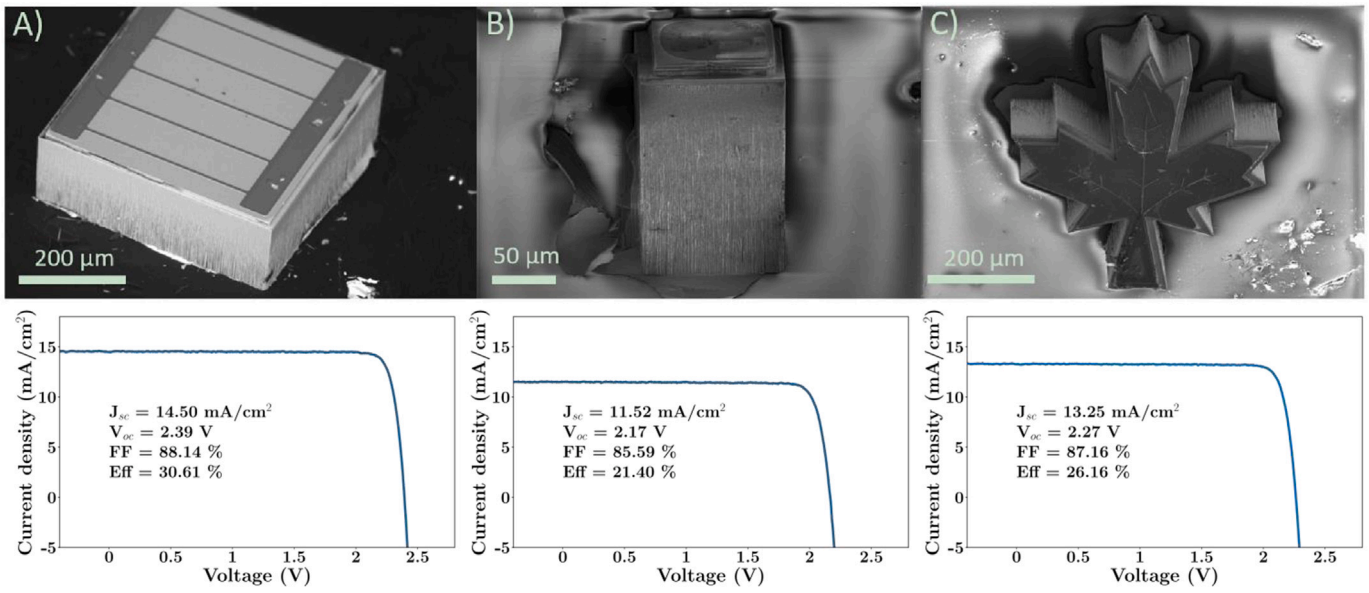

Fig. 1. SEM images of a 0.25 mm^2, 0.01 mm^2 and 0.081 mm^2 maple leaf cells after full singulation as well as their I–V measurements below each images respectively. The surface area used to normalize the current is the active surface area of the cell, i.e. the mesa surface area minus the metallization surface area.

been calculated and compared to experimental V_{oc}. The study of non-radiative recombinations sub-cell by sub-cell allows to find the sub-cell most affected by perimeter recombinations.

2. Microfabrication process of cells

Cells are fabricated from a commercial InGaP/InGaAs/Ge wafer. The first step is to deposit the front contact by evaporation of Pd/Ge/Ti/Pd/Al (50/100/50/50/1000 nm) [22,23]. This contact is known to have a low contact resistance on GaAs, which reduces problems of series resistance at high concentrations. Cells are then electrically isolated using $SiCl_4/Cl_2/H_2$ plasma etching [21]. This plasma chemistry is known to reduce perimeter effects and therefore improve V_{oc} on submillimeter cells [13,20,21]. The base contact is then deposited, on the back surface of the cell, by Ni/Au (50/200 nm) [20] evaporation. The contact layer is then etched with $NH_4OH/H_2O_2/H_2O$, which at the same time enables a wet cleaning process to increase the V_{oc} [19]. Then, an antireflective layer (SiN/SiO) is deposited by plasma enhanced chemical vapor deposition (PECVD) and opened at the contacts by CF_4 RIE plasma etching [13,24]. Plasma singulation is performed using a Bosch process consisting of several cycles alternating between SF_6/O_2 and C_4F_8 [25]. To ease the fabrication, a distance of 10 µm is chosen between the edge of the dicing line and the edge of the mesa. The dicing lines are 40 µm wide to achieve a compromise between kerf losses and etching time. This width enables kerf losses to be limited to around 15% [26] but can easily be reduced to less than 10% [27].

This process enables to manufacture solar cells of any size and shape. Square cells have been manufactured with sizes ranging from 12.25 mm^2 to 0.01 mm^2 as well as different shapes: round, triangular, maple leaf, hexagonal. Fig. 1 shows three types of cells fabricated, the cell in image (A) has a mesa surface of 0.25 mm^2. The one in image (B) has a mesa surface of 0.01 mm^2, to our knowledge, this is the smallest cell of its type ever made. The one in image (C) is a maple leaf-shaped cell of 0.081 mm^2 demonstrating the capability of plasma etching to fabricate versatile shapes of solar cells. In these images, it can be seen that the mesa size is close to the cell size, which limits material losses. Indeed, the mesa represent 93% of the cell size for 0.25 mm^2 cell and 70% for 0.01 mm^2 cell.

3. Electrical characterizations of cells

The electrical characteristics of the InGaP/InGaAs/Ge cells fabricated with the process described in the last section were measured with AM1.5D spectrum. The measurements were taken using a Newport SOL1 A solar simulator equipped with a 150 W Xenon lamp. The solar cells are connected with needle probes and the electrical measurements are made with a Keithley 2601 SMU. The assembly is also equipped with a TEC 2510 temperature controller. A reference cell is used to calibrate the lamp. One-sun measurements were carried out on cells ranging from 12.25 mm^2 to 0.01 mm^2.

Fig. 1 shows three I–V curves as well as performances for square cells of 0.25 mm^2 and 0.01 mm^2 and a maple leaf-shaped cell, as shown in SEM images above. We measured a record efficiency of 30.61% for the square 0.25 mm^2 cell. A 0.01 mm^2 cell was also measured, its efficiency reaches 21.40% but is severely limited by the J_{sc}. We measured an efficiency of 26.16% for the maple leaf-shaped cell, its J_{sc} is also a bit low. During the manufacture of these two samples, the anti reflective coating deposited was of poor quality, which reduced the J_{sc}. In addition, the corners of the cells were not properly protected during singulation, which explains the condition of certain corners of these two cells on the SEM images in Fig. 1 ((B) and (C)). These cells were not manufactured for their performance but to demonstrate the capabilities of plasma etching. Cell (A) in Fig. 1 and all the other measurements presented afterwards come from the same production with a good quality anti reflective coating.

The V_{oc} decreases linearly with the logarithm of the P/A ratio [13]. Fig. 2 shows the evolution of the V_{oc} as a function of P/A for our fabricated cell in blue and previous work in yellow and green [12,13]. For our results, several cells of each size were measured to produce an average for the V_{oc}, a table summarizing these data is available in Appendix A.2. The red and purple stars represent V_{oc} values for 3 × 3 mm^2 commercial cell and 0.85 mm^2 fabricated maple leaf shape cell respectively.

In Fig. 2, it can be observed that the V_{oc} of a 0.85 mm^2 maple leaf-shaped cell follows the same trend as for square cells. For a square cell with an equivalent surface area, the P/A would be 43 cm^{-1}, while it is 87 cm^{-1} in this case. This result confirms experimentally that the P/A ratio is the parameter of interest for studying perimeter recombination, regardless of size or shape. In Fig. 2 it appears that our 12.5 mm^2 cell has a V_{oc} equivalent to the state-of-the-art-commercial

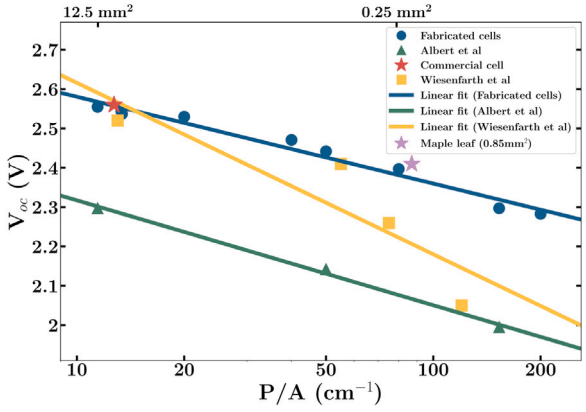

Fig. 2. Open circuit voltage (AM1.5D) as a function of perimeter-to-area ratio of fabricated cells, commercial cell and previous cells [12,13] The slope of fabricated cells is −0.094 V cm, the slope of Albert et al. is −0.116 V cm and the slope of Wiesenfarth et al. is −0.189 V cm.

cells. The V_{oc} measured for the commercial cell is 2.56 V compared to 2.55 V for our cell, which is of the same order of magnitude as the dispersions presented in the Appendix A.1. Fig. 2 shows that the V_{oc} of our laboratory-made cells are higher than previous studies for all cell sizes [9,13]. Moreover, the slope of the linear regression (on a semi-logarithmic scale) is larger for our cells: −0.094 V cm compared to −0.116 V cm for Albert et al. [13] and −0.189 V cm for Wiesenfarth et al. [12]. The larger slope indicates a lower sensitivity to perimeter effect, and therefore a lower perimeter recombination rate in comparison with previous work.

We have demonstrated the feasibility of fabricating cells with a decrease in V_{oc} relative to P/A of only −0.094 V cm. This result was obtained for 3J cells, for which it is complex to dissociate the sub-cells in series. However, to optimize passivation, we need to estimate which sub-cell suffers most from perimeter recombinations. In the remainder of this article, an assessment of V_{oc} losses sub-cell by sub-cell is done to specify which sub-cell is most sensitive to perimeter recombinations. To achieve this study, each sub-cell is manufactured independently for different sizes.

4. Microfabrication of sub-cells

To determine which sub-cell suffers the most from size reduction, we fabricated mono-junction of varying sizes from wafers identical to those used to obtain the cells described above. In this section, processes for the various mono-junctions are presented. These processes are derived from processes originally developed for multiterminal solar cells fabrication [28,29] and adapted to include plasma etching steps for junctions isolation.

For the top cell, the first step is to make the front contact by evaporation of Ni/Ge/Au/Ni/Au (45/30/90/30/100 nm) [20], shown in yellow in Fig. 3 (A) . Mesa etching is then carried out in two stages: a first step of plasma etching using the same process as for cell manufacture ($SiCl_4/Cl_2/H_2$) followed by selective H_3PO_4:HCl (1:4) [30] wet etching to etch down to the first tunnel junction. The plasma etching step is used first so that the sides of the sub-cell are isolated in the same way as the cells presented in previous section. The end of the etching is done by selective wet etching to stop precisely on the tunnel junction. A new photolithography step is performed to ensure that the sidewalls are protected by the photoresist during this wet etching. H_3PO_4:HCl (1:4) is known to etch P-containing layer (AlGaInP, InGaP and AlInP) selectively with GaAs-containing layer (GaAs, InGaAs and AlGaAs). This solution is therefore suitable for finishing the etching of the top cell (windows/emitted/BSF AlInP/InGaP/AlGaInP) selectively with the first tunnel junction in (AlGaAs) [28]. The base contact is then deposited on the tunnel junction by evaporation of Pt/Ti/Au (75/50/175 nm) [29], shown in light blue in Fig. 3 (A) .

For the middle cell, the top cell materials are first wet etched with H_2SO_4:H_2O_2:H_2O (1:10:20) [30] followed by H_3PO_4:HCl (1:4). Solution H_2SO_4:H_2O_2:H_2O (1:10:20) is known to etch GaAs-containing layers selectively to P-containing layers [28]. This solution enables to etch the cap layer and the solution H_3PO_4:HCl (1:4) etch the top cell until the first tunnel junction. The front contact of the middle sub-cell is made with the same metallization as the base contact of the top cell (Pt/Ti/Au (75/50/175 nm)), shown in light blue in Fig. 3 (B) . As with the top cell, the isolation stage begins with a plasma etching phase followed by a wet etch phase. Plasma etching is stopped in the middle cell base (InGaAs), solution H_2SO_4:H_2O_2:H_2O (1:10:20) allows to etch until the back surface field (BSF) (InGaP) which can then be etch with H_3PO_4:HCl (1:4) to expose the second tunnel junction. As for the top cell, the sidewalls are protected during the wet etching. The base contact of the middle sub-cell is then deposited by evaporation of Cu/Pt/Ti/Pt/Au (20/40/50/50/150 nm) [29], shown in orange in Fig. 3.

For the bottom cell, the top and the middle sub-cell materials are wet etched with solutions H_2SO_4:H_2O_2:H_2O (1:10:20) for GaAs-containing layer and H_3PO_4:HCl (1:4) for P-containing layer until the second tunnel junction. The front contact of the bottom sub-cell is then deposited by evaporation of Cu/Pt/Ti/Pt/Au (20/40/50/50/150 nm) as for the base contact of the middle sub-cell (orange in Fig. 3 (C)). Ni/Au (50/200 nm) evaporation is then carried out on the rear face of the germanium substrate to make the rear contact as presented in purple on Fig. 3 (C) . The isolation step is then entirely made by plasma.

With these process sequences, individual mono-junctions are therefore fabricated, with isolation processes as close as possible to the isolation process of the triple junction solar cell. It must be noticed that the upper cells are removed for the middle and bottom cell, meaning that the spectrum collected by the individual mono-junctions is not filtered out by the upper sub-cells, and is therefore different from the actual spectrum collected by each sub-cell in a triple junction solar cell. As a result, the V_{oc} of the middle cell and the bottom cell may be slightly overestimated compared with their operation in the triple junction cell. The contact layer has not been etched for mono-junction cells, which may lead to a slight underestimation of mono-junctions V_{oc}. It can also be noted that there is no optical coupling effect for the mono-junctions, and mono-junctions do not have an anti reflective coating, which could slightly lower their V_{oc} compared with their operation in the triple junction cell [13,31]. For these reasons, the sum of V_{oc} of mono-junction cells from Fig. 4 is underestimated by 3% to 7% compared to the V_{oc} of the 3J cell (Fig. 2). In comparison Albert et al. [13] found a difference of 2% to 5% for cells with and without ARC.

5. Electrical characterizations of sub-cells

Mono-junctions of different sizes were fabricated using the process described in the previous section. Measurements under one sun were carried out using the same equipment described in Section 3. V_{oc} as a function of P/A ratio is plotted for each mono-junction in Fig. 4. It can be seen that the sub-cell with the smallest slope is the top cell: −0.058 V cm compared to −0.022 V cm for the middle cell and −0.011 V cm for the bottom. This smaller slope means less passivation of the sides of the top cell and therefore greater perimeter effects for this sub-cell. By summing the V_{oc} of each mono-junction, the total V_{oc} is 5% to 6% lower than the result for a full cell shown in Fig. 1. There is a difference in V_{oc} as explained in the previous section. As for the slope, it is −0.092 mV cm (compared to −0.094 V cm in Fig. 1) in the case of the sum of the mono-junctions, confirming the same sidewalls passivation as for the triple junctions cells. Shunt resistance values are of the order of 10^5 ohm cm^2 for the top cell and 10^4 ohm cm^2 for the middle and bottom cells, and these values do not vary with size. V_{oc}

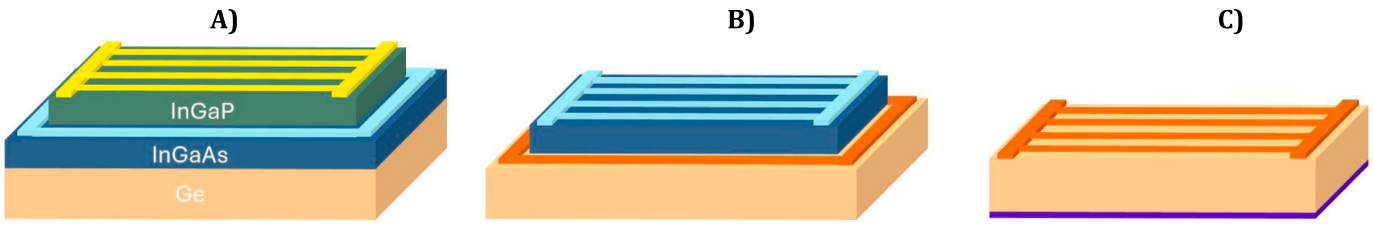

Fig. 3. Scheme of mono-junctions architecture (A) Top cell (B) Middle cell (C) Bottom cell. The yellow, light blue, orange, purple parts are respectively contacts made with: Ni/Ge/Au/Ni/Au (45/30/90/30/100 nm), Pt/Ti/Au (75/50/175 nm), Cu/Pt/Ti/Au (20/40/50/50/150 nm), Ni/Au (50/200 nm).

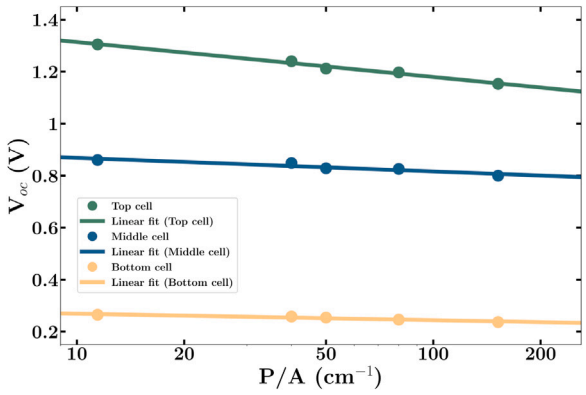

Fig. 4. Open circuit voltage as a function of perimeter-to-area ratio for each sub-cell. The slope of curves are −0.058 V cm, −0.022 V cm and −0.011 V cm for the top, middle and bottom cell respectively.

Table 1
Characteristics of our sub-cells, E_g comes from an EQE measurement, V_{oc}^{SQ} comes from Shockley–Queisser model, V_{oc}^{bulk} comes from Fig. 4 when P/A=1.

	Top cell	Middle cell	Bottom cell
E_g (eV)	1.8	1.33	0.67
V_{oc}^{SQ} (V)	1.49	1.03	0.42
V_{oc}^{bulk} (V)	1.448	0.921	0.294

is therefore unaffected by this resistance. Even though other methods exist for sub cells characteristics extraction [32], their applications to sub-millimetric cells are not straightforward due to the need for accurate and absolute EQE and electroluminescence measurements, that become very challenging at sub-millimeter scale. The following section looks at the evaluation of non-radiative losses in V_{oc}.

6. Summary of losses

In order to carry out a V_{oc} review of non-radiative losses on the cells. The theoretical V_{oc}^{SQ} of the cells is calculated using the Shockley–Queisser model (presented in Appendix A.1). This model only considers radiative losses, it will therefore be the point of comparison with measurements in order to evaluate non-radiative losses and in particular perimeter recombination losses. Table 1 shows the result of the Shockley–Queisser model as well as band gap values used, these values were found from EQE measurements.

With results from Fig. 4, we can define V_{oc}^{bulk}, the open circuit voltage of a 4 × 4 cm^2 (P/A=1) for which perimeter recombinations are considered negligible, values are presented in Table 1. Using the V_{oc}^{SQ} calculated and the V_{oc}^{bulk}, we are able to make a summary of non-radiative losses in V_{oc}. This summary is presented on Fig. 5.

In Fig. 5, it can be observed that the contribution of V_{oc} losses from non-radiative recombinations by excluding perimeter recombinations are increasingly important from the top cell to the bottom cell, with losses of 0.042 V, 0.109 V and 0.126 V for top cell, middle cell and bottom cell respectively. These losses are intrinsic to the substrate quality and the epitaxy used as well as to the contribution of the upper and lower surfaces.

As can be seen from a larger red surface area in Fig. 5, non-radiative losses at the perimeter dominate in the top cell for all size of cell fabricated. The top cell loses 0.251 V compared with 0.095 V for the middle cell and 0.048 V for the bottom cell for a cell of 0.25 mm^2 (P/A = 80 cm^{-1}). With these results, we can see that 64% of the losses related to perimeter recombination for a 0.25 mm^2 cell are in fact caused by the top cell. Delafontaine et al. [21] demonstrated an increase in the V_{oc} of solar cells by adding hydrogen to the plasma, which passivated the sides of the top cell only. This result confirms that this junction is the largest contributor for perimeter recombination losses and explains why the cells reported here and fabricated with the optimized plasma etching process present the lowest slope V_{oc} vs P/A reported in the literature for triple junction solar cells (Fig. 2). It must be noted that this result contradicts a study by Espinet Gonzalez et al. [17] that showed that perimeter recombination is dominated by the middle cell. However, a direct comparison is difficult since they carried out their own epitaxy and we used a commercial epitaxy for which we have very little information. In addition, the cell isolation method is not mentioned, which may strongly affect the losses due to perimeter recombinations. However, the precise reason why top cell perimeter recombinations dominated in the case of this commercial epitaxy remains unresolved. For the commercial epitaxial structure

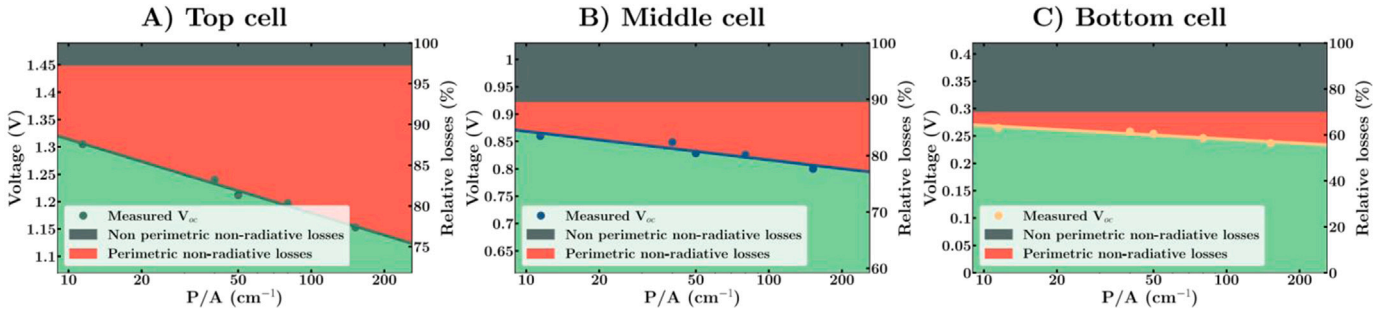

Fig. 5. Summary of losses in V_{oc} due to non-radiative recombination for (A) Top cell (B) Middle cell (C) Bottom cell. The voltage scale is kept constant (0.42 V as the V_{oc}^{SQ} of the bottom cell) so that the impact of losses on the complete cell can be visualized.

Table 2
Table of values used for Fig. 2.

P/A (cm^{-1})	11.43	13.33	13.38	20	40	50	80	153	200
Number of cell	2	2	2	4	18	9	75	10	3
Average V_{oc} (V)	2.555	2.544	2.537	2.53	2.472	2.442	2.398	2.297	2.283
$\mathbf{3\sigma V_{oc}}$	0.0015	0.012	0.0045	0.01662	0.02025	0.04494	0.03102	0.05952	0.00648

used there, the top cell is therefore the sub-cell to be passivated as a priority to further increase the performances of triple junction solar cells.

7. Conclusion

In this paper, we have fabricated InGaP/InGaAs/Ge solar cells with different size and shape with record V_{oc} of 2.39 V and 2.28 V for 0.25 mm^2 and 0.04 mm^2 cells respectively, indicating good sidewall passivation. We also investigated perimeter recombinations losses for each of the sub-cells. An assessment of losses through non-radiative recombination was carried out and showed that the top cell is the junction most affected by perimeter recombination. The top cell is therefore the junction that should be passivated as a priority to limit the drop in V_{oc} as cell size decrease. Finally, the balance of losses achieved will guide future research into improving multijunction cells in III–V materials.

CRediT authorship contribution statement

Corentin Jouanneau: Writing – review & editing, Writing – original draft, Visualization, Validation, Methodology, Investigation, Formal analysis, Data curation, Conceptualization. **Thomas Bidaud:** Visualization, Validation, Supervision, Methodology, Investigation, Formal analysis, Data curation, Conceptualization. **Paul Ferreol:** Investigation, Data curation. **Benjamin Breton:** Data curation. **Gwenaelle Hamon:** Supervision, Resources, Project administration, Funding acquisition. **Maxime Darnon:** Supervision, Resources, Project administration, Funding acquisition.

Declaration of competing interest

The authors declare that they have no known competing financial interests or personal relationships that could have appeared to influence the work reported in this paper.

Acknowledgments

LN2 is a joint international Research Laboratory (IRL 3463) funded and co-operated in Canada by Université de Sherbrooke (UDS) and in France by CNRS as well as ECL, INSA Lyon, and Université Grenoble Alpes (UGA). We acknowledge the support from NSERC (Canada), Prompt (Quebec) and STACE through the MARS-CPV project.

Appendix

A.1. Table of measurements in Fig. 2

See Table 2.

A.2. Theoretical open circuit voltage for each sub-cell

Since V_{oc} is the parameter of interest for characterizing micro-cells, we have calculated the V_{oc} for each sub-cells using the Shockley–Queisser model. This model only considers radiative recombinations. Using the theoretical V_{oc} and the measurements taken on the sub-cells, we can calculate the V_{oc} losses in each of the sub-cells.

The calculations are based on the assumptions of the Shockley–Queisser model. These assumptions are:

1- Perfect absorption for $E>E_g$, the absorptivity A(E) is a step function A(E)=0 for $E<E_g$ and A(E)=1 for $E>E_g$

2- An absorbed photon generate exactly one electron–hole pair which is collected at short circuit current (J_{sc}).

3- Thermalization towards E_c and E_v ($T_{carriers}=T_{cell}$ and $V_{ocmax} = \frac{E_g}{q}$),

4- Only radiative recombination (Black body emission at T_{cell} from the cell)

5- No ohmic losses, perfectly selective contacts (One contact recovers only electrons and the other the holes).

With these assumptions we can write the following formulas:

-From assumption 1 and 2, the J_{sc}^{SQ} (current gain) can be calculated using formula (1):

$$J_{sc}^{SQ} = q\int_{-\infty}^{+\infty} A(E)\phi_{inc}(E)dE \tag{1}$$

With q the electron charge, ϕ_{in} the incident photon flux.

-From assumption 3 and 4, J_0^{SQ} (current losses due to radiative recombinations) can be calculated using formula (2):

$$J_0^{SQ} = q\int_{-\infty}^{+\infty} A(E)\phi_{BB}(T_{cell},E)dE \tag{2}$$

With $\phi_{BB}(T_{cell})$ the emission flux of a black body at temperature T_{cell}

-From J_{sc}^{SQ} and J_0^{SQ} the J–V characteristic of a solar cell can be written as J_{sc}^{SQ} decreased by the diode current as in formula (3):

$$J^{SQ} = J_{sc}^{SQ} - J_0^{SQ}(ln(\frac{qV^{SQ}}{nkT_{cell}}) - 1) \tag{3}$$

With n the ideality factor (here n=1 because only radiative recombinations are taken in account), k the Boltzmann constant.

-From equation (3), the V_{oc} of a cell in the case of the Shockley–Queisser assumptions can be calculated with formula (4):

$$V_{oc}^{SQ} = \frac{kT_{cell}}{q} ln(\frac{J_{sc}^{SQ}}{J_0^{SQ}} + 1) \tag{4}$$

The band-gap values were determined from EQE measurements of our cells. The results of these measurements and calculations are summarized in Table 1.

Data availability

Data will be made available on request.

References

[1] M.A. Green, E.D. Dunlop, G. Siefer, M. Yoshita, N. Kopidakis, K. Bothe, X. Hao, Solar cell efficiency tables (Version 61), Prog. Photovolt., Res. Appl. 31 (2023) 3–16, http://dx.doi.org/10.1002/pip.3646.

[2] G.M. Wilson, M. Al-Jassim, W.K. Metzger, S.W. Glunz, P. Verlinden, G. Xiong, L.M. Mansfield, B.J. Stanbery, K. Zhu, Y. Yan, J.J. Berry, A.J. Ptak, F. Dimroth, B.M. Kayes, A.C. Tamboli, R. Peibst, K. Catchpole, M.O. Reese, C.S. Klinga, P. Denholm, M. Morjaria, M.G. Deceglie, J.M. Freeman, M.A. Mikofski, D.C. Jordan, G. TamizhMani, D.B. Sulas-Kern, The 2020 photovoltaic technologies roadmap, J. Phys. D: Appl. Phys. 53 (2020) 493001, http://dx.doi.org/10.1088/1361-6463/ab9c6a.

[3] Best Research-Cell Efficiency Chart, URL https://www.nrel.gov/pv/cell-efficiency.html.
[4] J.F. Geisz, R.M. France, K.L. Schulte, M.A. Steiner, A.G. Norman, H.L. Guthrey, M.R. Young, T. Song, T. Moriarty, Six-junction III–V solar cells with 47.1% conversion efficiency under 143 Suns concentration, Nat. Energy 5 (2020) 326–335, http://dx.doi.org/10.1038/s41560-020-0598-5.
[5] P. Schygulla, P. Beutel, S. Heckelmann, O. Höhn, M. Klitzke, J. Schön, E. Oliva, F. Predan, M. Schachtner, G. Siefer, H. Helmers, F. Dimroth, D. Lackner, Quadruple junction solar cell with 47.6 % conversion efficiency under concentration, 2022, URL https://publica.fraunhofer.de/handle/publica/436210.
[6] T. Takamoto, H. Washio, H. Juso, Application of InGaP/GaAs/InGaAs triple junction solar cells to space use and concentrator photovoltaic, in: 2014 IEEE 40th Photovoltaic Specialist Conference (PVSC), 2014, pp. 0001–0005, http://dx.doi.org/10.1109/PVSC.2014.6924936.
[7] C. Domínguez, N. Jost, S. Askins, M. Victoria, I. Antón, A review of the promises and challenges of micro-concentrator photovoltaics, in: AIP Conference Proceedings, Vol. 1881, 2017, 080003, http://dx.doi.org/10.1063/1.5001441.
[8] A. Ritou, P. Voarino, O. Raccurt, Does micro-scaling of CPV modules improve efficiency? A cell-to-module performance analysis, Sol. Energy 173 (2018) 789–803, http://dx.doi.org/10.1016/j.solener.2018.07.074.
[9] M. Wiesenfarth, D. Iankov, J.F. Martínez, P. Nitz, M. Steiner, F. Dimroth, H. Helmers, Technical boundaries of micro-CPV module components: How small is enough? AIP Conf. Proc. 2550 (2021) 030008, http://dx.doi.org/10.1063/5.0099878.
[10] O. Fidaner, F.A. Suarez, M. Wiemer, V.A. Sabnis, T. Asano, A. Itou, D. Inoue, N. Hayashi, H. Arase, A. Matsushita, T. Nakagawa, High efficiency micro solar cells integrated with lens array, Appl. Phys. Lett. 104 (2014) 103902, http://dx.doi.org/10.1063/1.4868116.
[11] A. Vossier, B. Hirsch, E.A. Katz, J.M. Gordon, On the ultra-miniaturization of concentrator solar cells, Sol. Energy Mater. Sol. Cells 95 (2011) 1188–1192, http://dx.doi.org/10.1016/j.solmat.2010.12.053.
[12] M. Wiesenfarth, M. Steiner, H. Helmers, A.W. Bett, Voltage losses due to the perimeter and dark area in micro-concentrator solar cells, Sol. Energy Mater. Sol. Cells 219 (2021) 110791, http://dx.doi.org/10.1016/j.solmat.2020.110791.
[13] P. Albert, A. Jaouad, G. Hamon, M. Volatier, C.E. Valdivia, Y. Deshayes, K. Hinzer, L. Béchou, V. Aimez, M. Darnon, Miniaturization of InGaP/InGaAs/Ge solar cells for micro-concentrator photovoltaics, Prog. Photovolt., Res. Appl. 29 (2021) 990–999, http://dx.doi.org/10.1002/pip.3421.
[14] A. Itou, T. Asano, D. Inoue, H. Arase, A. Matsushita, N. Hayashi, R. Futakuchi, K. Inoue, M. Yamamoto, E. Fujii, T. Nakagawa, Y. Anda, H. Ishida, T. Ueda, O. Fidaner, M. Wiemer, D. Ueda, High-efficiency thin and compact concentrator photovoltaics using micro-solar cells with via-holes sandwiched between thin lens-array and circuit board, Japan. J. Appl. Phys. 53 (2014) 04ER01, http://dx.doi.org/10.7567/JJAP.53.04ER01.
[15] N. Hayashi, D. Inoue, M. Matsumoto, A. Matsushita, H. Higuchi, Y. Aya, T. Nakagawa, High-efficiency thin and compact concentrator photovoltaics with micro-solar cells directly attached to a lens array, Opt. Express 23 (2015) A594–A603, http://dx.doi.org/10.1364/OE.23.00A594.
[16] N. Hayashi, A. Matsushita, D. Inoue, M. Matsumoto, T. Nagata, H. Higuchi, Y. Aya, T. Nakagawa, Nonuniformity sunlight-irradiation effect on photovoltaic performance of concentrating photovoltaic using microsolar cells without secondary optics, IEEE J. Photovoltaics 6 (2016) 350–357, http://dx.doi.org/10.1109/JPHOTOV.2015.2491598.
[17] P. Espinet-González, I. Rey-Stolle, M. Ochoa, C. Algora, I. García, E. Barrigón, Analysis of perimeter recombination in the subcells of GaInP/GaAs/Ge triple-junction solar cells, Prog. Photovolt., Res. Appl. 23 (2015) 874–882, http://dx.doi.org/10.1002/pip.2501.
[18] M. Ochoa, C. Algora, P. Espinet-González, I. García, 3-D modeling of perimeter recombination in GaAs diodes and its influence on concentrator solar cells, Sol. Energy Mater. Sol. Cells 120 (2014) 48–58, http://dx.doi.org/10.1016/j.solmat.2013.08.009.
[19] M.d. Lafontaine, F. Ayari, E. Pargon, G. Gay, C. Petit-Etienne, A. Turala, A. Jaouad, M. Volatier, S. Fafard, V. Aimez, M. Darnon, Multijunction solar cell mesa isolation: A comparative study, in: AIP Conference Proceedings, Vol. 2550, 2022, 020003, http://dx.doi.org/10.1063/5.0099529.
[20] M. de Lafontaine, E. Pargon, C. Petit-Etienne, G. Gay, A. Jaouad, M.-J. Gour, M. Volatier, S. Fafard, V. Aimez, M. Darnon, Influence of plasma process on III-V/Ge multijunction solar cell via etching, Sol. Energy Mater. Sol. Cells 195 (2019) 49–54, http://dx.doi.org/10.1016/j.solmat.2019.01.048.
[21] M. de Lafontaine, E. Pargon, G. Gay, C. Petit-Etienne, S. David, J.-P. Barnes, N. Rochat, A. Jaouad, M. Volatier, S. Fafard, V. Aimez, M. Darnon, Anisotropic and low damage III-V/Ge heterostructure etching for multijunction solar cell fabrication with passivated sidewalls, Micro Nano Eng. 11 (2021) 100083, http://dx.doi.org/10.1016/j.mne.2021.100083.
[22] P. Huo, I. Rey-Stolle, Al-based front contacts for HCPV solar cell, in: AIP Conference Proceedings, Vol. 1881, 2017, 040004, http://dx.doi.org/10.1063/1.5001426.
[23] O. Richard, A. Turala, V. Aimez, M. Darnon, A. Jaouad, Low-cost passivated Al front contacts for III-V/Ge multijunction solar cells, Energies 16 (2023) 6209, http://dx.doi.org/10.3390/en16176209.
[24] R. Homier, A. Jaouad, A. Turala, C.E. Valdivia, D. Masson, S.G. Wallace, S. Fafard, R. Ares, V. Aimez, Antireflection coating design for triple-junction III–V/Ge high-efficiency solar cells using low absorption PECVD silicon nitride, IEEE J. Photovoltaics 2 (3) (2012) 393–397, http://dx.doi.org/10.1109/JPHOTOV.2012.2198793.
[25] M. Darnon, M. de Lafontaine, M. Volatier, S. Fafard, R. Arès, A. Jaouad, V. Aimez, Deep germanium etching using time multiplexed plasma etching, J. Vac. Sci. Technol. B 33 (2015) 060605, http://dx.doi.org/10.1116/1.4936112.
[26] C. Jouanneau, T. Bidaud, A. Turala, D. Danovitch, G. Hamon, M. Darnon, A novel parallel interconnection approach to reduce shading losses on submillimeter concentrated photovoltaic technologies, in: 2024 IEEE 74th Electronic Components and Technology Conference (ECTC), 2024, pp. 2205–2210, http://dx.doi.org/10.1109/ECTC51529.2024.00375.
[27] M. Darnon, M.d. Lafontaine, P. Albert, C. Jouanneau, T. Bidaud, C. Dubuc, M. Volatier, V. Aimez, A. Jaouad, G. Hamon, Sub-millimeter-scale multijunction solar cells for concentrator photovoltaics (CPV), in: Physics, Simulation, and Photonic Engineering of Photovoltaic Devices XI, Vol. 11996, 2022, pp. 49–58, http://dx.doi.org/10.1117/12.2613441.
[28] T. Bidaud, F. Ayari, P. Ferreol, C. Jouanneau, A. Turala, S. Moreau, M. Volatier, V. Aimez, S. Fafard, A. Jaouad, M. Darnon, G. Hamon, Multi-terminal GaInP/GaInAs/Ge solar cells for subcells characterization, Energies 17 (2024) 2538, http://dx.doi.org/10.3390/en17112538.
[29] F. Ayari, S. Moreau, M.D. Lafontaine, A. Turala, G. Hamon, T. Bidaud, M. Volatier, V. Aimez, A. Jaouad, M. Darnon, Multi-terminal three-junction solar cells for sub-cells characterization, in: 18th Conference on Concentrated PhotoVoltaïcs System, 2022.
[30] A.R. Clawson, Guide to references on III–V semiconductor chemical etching, Mater. Sci. Eng. R 31 (2001) 1–438, http://dx.doi.org/10.1016/S0927-796X(00)00027-9.
[31] M.A. Steiner, J.F. Geisz, Non-linear luminescent coupling in series-connected multijunction solar cells, Appl. Phys. Lett. 100 (2012) 251106, http://dx.doi.org/10.1063/1.4729827.
[32] S. Roensch, R. Hoheisel, F. Dimroth, A.W. Bett, Subcell I-V characteristic analysis of GaInP/GaInAs/Ge solar cells using electroluminescence measurements, Appl. Phys. Lett. 98 (2011) 251113, http://dx.doi.org/10.1063/1.3601472.